symmetry

IMPACT FACTOR 2.7

CITESCORE 4.9

Article

Radiative Effects in Low-Dimensional Effective Fermion Field Theory with Compactification

Vladimir Ch. Zhukovsky

MDPI

https://doi.org/10.3390/sym15101867

symmetry

MDPI

Article

Radiative Effects in Low-Dimensional Effective Fermion Field Theory with Compactification

Vladimir Ch. Zhukovsky

Faculty of Physics, Department of Theoretical Physics, Moscow State University, 119899 Moscow, Russia; vlchzh@gmail.com

Abstract: The introduction of branes immersed in the space-times of higher dimensions revealed itself to be a useful instrument for the study of high-dimensional models in quantum field theory. Moreover, low-dimensional quantum field theories represent an especially interesting class of models in physics due to their unique properties and renormalizability when interactions are treated perturbatively. The advantages of both approaches can be combined in a model for a low-dimensional brane immersed in the usual tetradimensional Minkowski space-time, the properties of which are relatively well known. This approach can be used for the study of systems like graphene and carbon nanotubes. In the present work, we present an effective model for nanotubes based on the Lagrangian obtained from a tight-binding model for graphene. The induced current, appearing azimuthally in the presence of a magnetic flux through the tube section (Aharonov–Bohm effect), will be derived. A reduced Lagragian for photons confined on the tube surface, obtained from the literature, is included in the last part of the work to threat perturbative corrections to the induced current.

Keywords: Aharonov–Bohm effect; graphene; carbon nanotubes

check for updates

Citation: Zhukovsky, V.C. Radiative Effects in Low-Dimensional Effective Fermion Field Theory with Compactification. *Symmetry* **2023**, *15*, 1867. https://doi.org/10.3390/sym15101867

Academic Editor: Sergei D. Odintsov

Received: 18 August 2023
Revised: 26 September 2023
Accepted: 28 September 2023
Published: 4 October 2023

Copyright: © 2023 by the author. Licensee MDPI, Basel, Switzerland. This article is an open access article distributed under the terms and conditions of the Creative Commons Attribution (CC BY) license (https://creativecommons.org/licenses/by/4.0/).

1. Introduction

Relativistic quantum field theory provides a powerful tool for the description of low-energy excitations in condensed-matter physics [1,2], with some of the examples being the field theoretic description of low-energy electron states in polymers [3–5]. In the case of graphene, a planar two-dimensional layer of sp^2-hybridized carbon, the respective low-energy quantum field theory Lagrangian can be obtained from a nonrelativistic tight-binding model for electrons on a hexagonal "honeycomb" lattice [6–8]. This results in an effective Dirac equation for massless fermions in $2+1$ Minkowski space-time [9].

The model obtained by "rolling up" the graphene sheet around a given axis enables the description of a closely related class of materials—the carbon nanotubes. For nanotubes of sufficiently large diameters, the energy structure may be obtained by simply imposing periodic conditions on the graphene wavefunctions along the circumference direction [10]. As a result of various possibilities of rolling up the graphene sheet, the band structure for a given nanotube may or may not conserve the zero-gap conductive properties of planar graphene [11]. The presence of an external magnetic field parallel to the tube axis may result in the appearance of induced electrical currents through the walls of nanotubes. Since the interaction with the electrons from the nanotube are mediated directly by the classical vector potential, the problem may be reduced to the analysis of the Aharonov–Bohm effect [12]. Phase transitions in hexagonal, graphene-like lattice sheets and nanotubes under the influence of external conditions were discussed in reference [13]. Graphene, under the influence of the Aharonov–Bohm flux and a constant magnetic field, was studied in reference [14]. Besides the magnetic flux through the nanotubes, other parameters expected to considerably affect the behaviour of induced currents are temperature and chemical potential. The effective potential derived from the generating functional for a nanotube can account for all three aforementioned effects and provides a simple path for

calculating the generated current in this system. In this sense, a thorough derivation of the induced current based on, finite-temperature quantum field theory formalism, is proposed in this work.

Experimental measurements of the electrical resistivity in nanotubes immersed in external magnetic fields show that the measured quantity approximately oscillates periodically with the intensity of the magnetic flux [15,16]. Temperature increase was revealed to lower the intensity of the oscillations, without considerably affecting the periods. The oscillating behavior of the resistivity was accompanied, in some cases, by minor oscillations, which could not be proved to be mere detector noise [15]. It was supposed by the authors that the minor oscillations are due to the mechanical stretching of the nanotubes that favor some given winding numbers for closed electron trajectories encircling the tube. It is believed that the presence of those oscillations may also be triggered by other physical effects, the contributions of which should be some orders of magnitude lower than the gross resistivity. This is exactly what happens in quantum field theories when accounting for interactions perturbatively. Following this reasoning, the perturbative treatment of interactions between fermions and generated photons, both confined to the nanotubes, were included in the calculation of the induced current to account for possible minor oscillations. The reduction of the photons Lagrangian in 3 + 1 Minkowski space-time to a Lagrangian in 2 + 1 dimensions can be realized following the proposal of Gusynin et al. [17].

2. Effective Low-Energy Model

2.1. The Tight-Binding Model for Graphene and the Transition to Quantum Field Theory

Graphene's hexagonal lattice can be described in terms of two triangular sublattices, say A and B. Each hexagonal unit cell contains two atoms, one from each sublattice [9]. Let $a = 1.42$ Å be the C-C bond length in graphene, then the vectors connecting nearest neighboring atoms from the same ($\vec{a}_1$ and $\vec{a}_2$) and different sublattices ($\vec{\delta}_1$, $\vec{\delta}_2$ and $\vec{\delta}_3$) can be represented as follows (see Figure 1):

$$\vec{a}_1 = \left(\frac{\sqrt{3}a}{2}, \frac{3a}{2}\right), \quad \vec{a}_2 = \left(\frac{\sqrt{3}a}{2}, -\frac{3a}{2}\right), \quad \vec{\delta}_1 = (0, a), \quad \vec{\delta}_2 = \left(\frac{\sqrt{3}a}{2}, -\frac{a}{2}\right), \quad \vec{\delta}_3 = \left(-\frac{\sqrt{3}a}{2}, -\frac{a}{2}\right). \tag{1}$$

Starting from any given atom in the lattice, any other atom of the same sublattice can be achieved by a translation of the kind $\vec{n}_{A,B} = n_1\vec{a}_1 + n_2\vec{a}_2$, with $n_1, n_2 \in \mathbb{Z}$. In the chosen representation, the reciprocal vectors, defined by the relation $\vec{a}_i \cdot \vec{b}_j = 2\pi\delta_{ij}$, are given as follows (see Figure 1):

$$\vec{b}_1 = \frac{2\pi}{\sqrt{3}a}\left(1, \frac{1}{\sqrt{3}}\right), \quad \vec{b}_2 = \frac{2\pi}{\sqrt{3}a}\left(1, -\frac{1}{\sqrt{3}}\right). \tag{2}$$

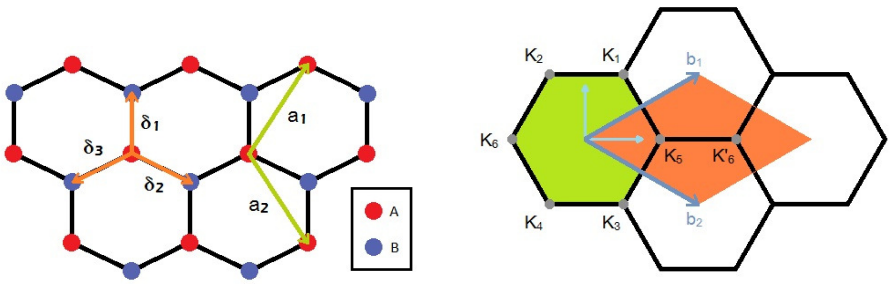

Figure 1. Left: Graphene's hexagonal lattice with labeled sublattices A and B and its main vectors. **Right**: Graphene's reciprocal lattice. The reference system of coordinates in the momentum space is represented by the blue arrows in the center of the green hexagon. The Brillouin zone (BZ) is represented by the green hexagon, in the vertices of which the points (9) are located. The expanded Brillouin zone is shown as an orange rhombus containing the points $\vec{K}_5 = \vec{K}$ and $\vec{K}'_6 \sim \vec{K}'$.

Since, for each carbon atom in graphene, three of the four valence electrons form σ-bonds with neighboring atoms through sp^2-hybridized orbitals, the remaining electrons from $2p_z$ orbitals are the only ones contributing to the formation of delocalized π-bonds. Therefore, in the simplest description of the tight-binding model for graphene, only the latter electrons should be accounted for [9]:

$$\hat{H} = -t \sum_{\vec{n},j,\sigma} \left[\hat{a}^{\dagger}_{\vec{n},\sigma} e^{-ie\vec{\delta}_j \cdot \vec{A}} \hat{b}_{\vec{n}+\vec{\delta}_j,\sigma} + \hat{b}^{\dagger}_{\vec{n}+\vec{\delta}_j,\sigma} e^{ie\vec{\delta}_j \cdot \vec{A}} \hat{a}_{\vec{n},\sigma} \right] + \frac{1}{3} \sum_{\vec{n},j,\sigma} eA_0 \left[\hat{a}^{\dagger}_{\vec{n},\sigma} \hat{a}_{\vec{n},\sigma} + \hat{b}^{\dagger}_{\vec{n}+\vec{\delta}_j,\sigma} \hat{b}_{\vec{n}+\vec{\delta}_j,\sigma} \right], \quad (3)$$

where t is the hopping integral between nearest neighboring atoms (from different sublattices), which was chosen as a constant due to the symmetry of the system. Here, $\hat{a}^{\dagger}_{\vec{n},\sigma}$ and $\hat{a}_{\vec{n},\sigma}$ are the creation and anihilation operators for electrons with spin σ in the site $\vec{n}$ of the sublattice A, while $\hat{b}^{\dagger}_{\vec{n}+\vec{\delta}_j,\sigma}$ and $\hat{b}_{\vec{n}+\vec{\delta}_j,\sigma}$ are the creation and anihilation operators for electrons with spin σ in the site $\vec{n}+\vec{\delta}_j$ of the sublattice B, respectively. The vector potential $\vec{A}$ was introduced in the Hamiltonian through Peierls substitution, assuming that $\vec{A}$ is a slowly varying function of $\vec{x}$. Here, and throughout this work, a natural system of units is used ($\hbar = c = k_B = 1$) and the charge of the electron is set as $e = -|e|$ [18]. Expanding the Peierls exponent as a Taylor series up to the term of first order in $\vec{A}$, one obtains $\hat{H}$ as a sum of the free Hamiltonian $\hat{H}_0$ and an interaction term $\sum_{\vec{n}} e\vec{A} \cdot \vec{j}$, where

$$\vec{j} = it \sum_{j,\sigma} \vec{\delta}_j \left(\hat{a}^{\dagger}_{\vec{n},\sigma} \hat{b}_{\vec{n}+\vec{\delta}_j,\sigma} - \hat{b}^{\dagger}_{\vec{n}+\vec{\delta}_j,\sigma} \hat{a}_{\vec{n},\sigma} \right), \quad (4)$$

$$\hat{H}_0 = -t \sum_{\vec{n},j,\sigma} \left[\hat{a}^{\dagger}_{\vec{n},\sigma} \hat{b}_{\vec{n}+\vec{\delta}_j,\sigma} + \hat{b}^{\dagger}_{\vec{n}+\vec{\delta}_j,\sigma} \hat{a}_{\vec{n},\sigma} \right]. \quad (5)$$

The above expressions expressions can be obtained in momentum space by using a Fourier transform of the form

$$\begin{pmatrix} \hat{a}_{\vec{n},\sigma} \\ \hat{b}_{\vec{n}+\vec{\delta}_j,\sigma} \end{pmatrix} = \sum_{\vec{k} \in \mathrm{BZ}} e^{i\vec{k}\cdot\vec{n}} \begin{pmatrix} \hat{a}_{\vec{k},\sigma} \\ e^{i\vec{k}\cdot\vec{\delta}_j} \cdot \hat{b}_{\vec{k},\sigma} \end{pmatrix}, \quad (6)$$

where the sum runs over the points of the expanded Brillouin Zone, which is formed by the vectors (2).

By making the transition to continuous momenta, the free Hamiltonian can be expressed by a formula similar to the one used in the second quantization formalism

$$\hat{H}_0 = S \sum_{\sigma} \int_{\mathrm{BZ}} \hat{\psi}^{\dagger}_{\sigma}(\vec{k}) \hat{\mathcal{H}}'_0 \hat{\psi}_{\sigma}(\vec{k}) \frac{\mathrm{d}^2 k}{(2\pi)^2}, \quad \text{with} \quad \hat{\mathcal{H}}'_0(\vec{k}) = \begin{pmatrix} 0 & \phi(\vec{k}) \\ \phi^*(\vec{k}) & 0 \end{pmatrix} \quad \text{and} \quad \hat{\psi}_{\sigma}(\vec{k}) = \begin{pmatrix} \hat{a}_{\sigma}(\vec{k}) \\ \hat{b}_{\sigma}(\vec{k}) \end{pmatrix}, \quad (7)$$

where $\phi(\vec{k}) = -t \sum_j e^{i\vec{k}\cdot\vec{\delta}_j}$, and $S = 3\sqrt{3}a^2/2$ is the area of a unit cell.

The diagonalization of $\hat{\mathcal{H}}'_0$ gives the energy eigenvalues for this system:

$$E_{\pm} = \pm t \sqrt{1 + 4\cos\left(\frac{\sqrt{3}}{2} a k_1\right) \cos\left(\frac{3}{2} a k_2\right) + 4\cos^2\left(\frac{\sqrt{3}}{2} a k_1\right)}. \quad (8)$$

Since graphene contains two atoms per unit cell, the dispersion relation gives two energy bands, one for quasiparticles with positive energies and other for quasiparticles with negative energies, as shown in Figure 2.

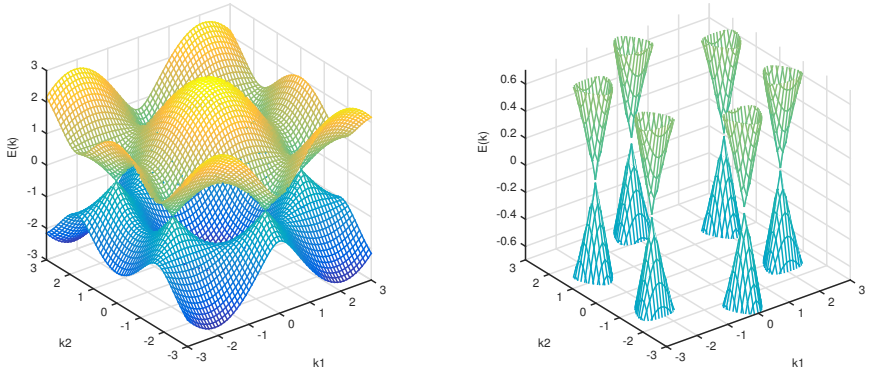

Figure 2. Left: Energy distribution in graphene as a function of the reciprocal coordinates (in units of $1/a$). **Right**: Behavior of the energy distribution close to the points (9). The energy is given in units of t.

In the Brillouin Zone, there are six points for which $\phi(\vec{k})$ goes to zero, so that the energy gap between the valence and conduction bands vanishes:

$$\begin{aligned} \vec{K}_1 &= \tfrac{2\pi}{a}\left(\tfrac{1}{3\sqrt{3}}, \tfrac{1}{3}\right), \quad \vec{K}_2 = \tfrac{2\pi}{a}\left(-\tfrac{1}{3\sqrt{3}}, \tfrac{1}{3}\right), \quad \vec{K}_3 = \tfrac{2\pi}{a}\left(\tfrac{1}{3\sqrt{3}}, -\tfrac{1}{3}\right), \\ \vec{K}_4 &= \tfrac{2\pi}{a}\left(-\tfrac{1}{3\sqrt{3}}, -\tfrac{1}{3}\right), \quad \vec{K}_5 = \tfrac{2\pi}{a}\left(\tfrac{2}{3\sqrt{3}}, 0\right), \quad \vec{K}_6 = \tfrac{2\pi}{a}\left(-\tfrac{2}{3\sqrt{3}}, 0\right). \end{aligned} \tag{9}$$

These six points represent the vertices of a unit cell in the reciprocal space (Brillouin Zone). In the vicinity of any of these points, the dispersion relation for the energy can be approximately expressed as a linear function of $|\vec{p}|$:

$$E_{\pm}(\vec{K}_i + \vec{p}) \approx \pm\frac{3at}{2}|\vec{p}| = \pm v_F|\vec{p}| \qquad |\vec{p}| \ll |\vec{K}_i|, \tag{10}$$

where $\vec{K}_i$ represents any of the points (9), $|\vec{p}|$ is the norm of the momentum vector calculated from this point and v_F is the Fermi velocity.

As a consequence of the hexagonality of graphene's reciprocal lattice, only two non-nearest neighboring points from (9) are actually non-equivalent; for that reason, in what follows, the analysis will be restricted to the points $\vec{K} = \vec{K}_5 = \frac{2\pi}{a}\left(\frac{2}{3\sqrt{3}}, 0\right)$ and $\vec{K}' = \vec{K}_6 = \frac{2\pi}{a}\left(-\frac{2}{3\sqrt{3}}, 0\right)$, which are called Dirac points (DP). In the vicinity of points $\vec{K}$ and $\vec{K}'$ the function $\phi(\vec{k})$ can be approximated by

$$\begin{cases} \phi(\vec{K} + \vec{p}) \approx +v_F(p_1 - ip_2) \\ \phi(\vec{K}' + \vec{p}) \approx -v_F(p_1 + ip_2) \end{cases},$$

as a consequence of which the free Hamiltonian can be written as follows:

$$\begin{aligned} \hat{H}_0 \approx S\sum_\sigma \int_{\mathrm{DP}} \Big\{ &\hat{\psi}^\dagger_\sigma(\vec{K} + \vec{p})[v_F(\tau_1 p_1 + \tau_2 p_2)]\hat{\psi}_\sigma(\vec{K} + \vec{p}) + \\ &\hat{\psi}^\dagger_\sigma(\vec{K}' + \vec{p})[-v_F(\tau_1 p_1 - \tau_2 p_2)]\hat{\psi}_\sigma(\vec{K}' + \vec{p}) \Big\} \frac{\mathrm{d}^2 p}{(2\pi)^2}. \end{aligned} \tag{11}$$

The spinors $\hat{\psi}_\sigma(\vec{K} + \vec{p})$ and $\hat{\psi}_\sigma(\vec{K}' + \vec{p})$ can be combined into a single spinor of the form

$$\hat{\Psi}_\sigma(\vec{p}) = \begin{pmatrix} \hat{a}_\sigma(\vec{K} + \vec{p}) \\ \hat{b}_\sigma(\vec{K} + \vec{p}) \\ \hat{b}_\sigma(\vec{K}' + \vec{p}) \\ \hat{a}_\sigma(\vec{K}' + \vec{p}) \end{pmatrix}, \tag{12}$$

which allows one to write $\hat{H}_0$ as a Dirac's Hamiltonian in the second quantization formalism (with integration in the momentum space running over the points in the vicinity of $\vec{K}$ and $\vec{K}'$):

$$\hat{H}_0 \approx S\sum_{\sigma}\int_{\mathrm{DP}} \hat{\Psi}^{\dagger}_{\sigma}(\vec{p})\hat{\mathcal{H}}_0(\vec{p})\hat{\Psi}_{\sigma}(\vec{p})\frac{\mathrm{d}^2p}{(2\pi)^2}\,, \quad \hat{\mathcal{H}}_0(\vec{p}) = v_F\gamma^0\left(\gamma^1 p_1 + \gamma^2 p_2\right). \tag{13}$$

Here, and throughout this work, the 4×4 Dirac matrices γ^{μ} ($\mu = \overline{0,3}$) are chosen in the following block representation:

$$\gamma^0 = \begin{pmatrix} 0 & 1_2 \\ 1_2 & 0 \end{pmatrix}, \qquad \gamma^i = \begin{pmatrix} 0 & -\tau^i \\ \tau^i & 0 \end{pmatrix}, \qquad \gamma^5 = \begin{pmatrix} 1_2 & 0 \\ 0 & -1_2 \end{pmatrix}. \tag{14}$$

A similar procedure can be used to convert the interaction terms from the tight-binding model into their respective quantum field theory counterparts. From Equation (4), and accounting for the slow variation of $\vec{A}$, one obtains

$$\sum_{\vec{n}}\vec{A}\cdot\vec{j} \approx tS\sum_{j,\sigma}\int \hat{\psi}^{\dagger}_{\sigma}(\vec{k})\left[\lim_{\vec{k}'\to\vec{k}}\vec{A}\cdot\frac{\partial}{\partial\vec{k}'}\begin{pmatrix} 0 & e^{i\vec{k}'\cdot\vec{\delta}_j} \\ e^{-i\vec{k}'\cdot\vec{\delta}_j} & 0 \end{pmatrix}\right]\hat{\psi}_{\sigma}(\vec{k})\frac{\mathrm{d}^2k}{(2\pi)^2}\,, \tag{15}$$

which results in the following approximation:

$$\sum_{\vec{n}}\vec{A}\cdot\vec{j} \approx -v_F S\sum_{\sigma}\int_{\mathrm{DP}}\hat{\overline{\Psi}}_{\sigma}(\vec{p})\vec{A}\cdot\vec{\gamma}\hat{\Psi}_{\sigma}(\vec{p})\frac{\mathrm{d}^2p}{(2\pi)^2}\,, \tag{16}$$

where $\hat{\overline{\Psi}}_{\sigma} = \hat{\Psi}^{\dagger}_{\sigma}\gamma^0$. The interaction with the electrostatic potential can be handled in an analogous way.

$$\sum_{\vec{n}} eA_0(\hat{N}_A + \hat{N}_B) \approx S\sum_{\sigma}\int_{\mathrm{DP}}\hat{\overline{\Psi}}_{\sigma}(\vec{p})eA_0\gamma^0\hat{\Psi}_{\sigma}(\vec{p})\frac{\mathrm{d}^2p}{(2\pi)^2}\,. \tag{17}$$

As a result, the final form of the quantum mechanical Hamiltonian and Lagrangian operators are as follows:

$$\hat{\mathcal{H}} = -iv_F\gamma^0\left(\gamma^1\partial_1 + \gamma^2\partial_2 - ie\vec{\gamma}\cdot\vec{A}\right) + eA_0\,, \tag{18}$$

$$\mathcal{L} = \sum_{\sigma}\Psi^{\dagger}_{\sigma}(t,\vec{x})\left[i\partial_0 - \hat{\mathcal{H}}(\vec{x})\right]\Psi_{\sigma}(t,\vec{x}) = \sum_{\sigma}\overline{\Psi}_{\sigma}(x)\left[i\gamma^{\alpha}\widetilde{D}_{\alpha}\right]\Psi_{\sigma}(x)\,, \tag{19}$$

where $\widetilde{D}_{\alpha} = (\partial_0 + ieA_0, v_F\vec{\partial} - iev_F\vec{A})$ and the index α runs from zero to two. Despite the evident similarity between Dirac's Lagrangian for free fermions in Minkowski space-time, and the obtained Lagrangian for fermions in graphene, field functions $\Psi(\vec{x})$ and $\overline{\Psi}(\vec{x})$ above contain eight components each, if one accounts for the two spin degrees of freedom.

2.2. Nanotubes from Graphene

The structure of nanotubes, ignoring their tips, can be obtained by "rolling up" graphene sheets around a given axis. Carbon nanotubes can be synthesized as either single-walled or multiwalled concentric tubular structures, and their diameters vary approximately from 7 Å to 300 Å [19]. Since, for multiwalled nanotubes, the distance between adjacent layers (∼3.4 Å) is considerably larger than the distance between nearest neighboring atoms from the same layer (∼1.4 Å), the electronic properties of such materials are mainly determined by the properties of single-walled nanotubes [10,20,21].

The direction, along which the graphene sheet should be rolled to form a carbon nanotube, is given by the chiral vector:

$$\vec{L} = l_1\vec{a}_1 + l_2\vec{a}_2 = \left(\frac{\sqrt{3}a}{2}[l_1 + l_2], \frac{3a}{2}[l_1 - l_2]\right), \qquad l_1, l_2 \in \mathbb{Z}, \tag{20}$$

which is chosen so that the carbon atom at $\vec{L}$ is superimposed on the atom lying at the origin. The length of the chiral vector determines the circumference of the tube:

$$L = \sqrt{3}a\left[l_1^2 + l_2^2 - l_1 l_2\right]^{1/2}. \tag{21}$$

The translation vector along the axis of the tube is given by

$$\vec{T} = m_1\vec{a}_1 + m_2\vec{a}_2 = \left(\frac{\sqrt{3}a}{2}[m_1 + m_2], \frac{3a}{2}[m_1 - m_2]\right), \qquad m_1, m_2 \in \mathbb{Z}, \tag{22}$$

and is determined by the relation $\vec{T}\cdot\vec{L} = 0$, which leads to the following constraints on the possible (integer) values of m_1 and m_2:

$$m_1(2l_1 - l_2) - m_2(l_1 - 2l_2) = 0. \tag{23}$$

Equation (23) admits solutions of the form $dm_1 = l_1 - 2l_2$ and $dm_2 = 2l_1 - l_2$, where d is the greatest common divisor of $l_1 - 2l_2$ and $2l_1 - l_2$. The length of $\vec{T}$ is given by a formula analogous to the expression (21) for $\vec{L}$ with $l_i \to m_i$.

The unit cell of a nanotube consists of a rectangular section of the graphene sheet formed by the vectors $\vec{L}$ and $\vec{T}$:

$$S_{\mathrm{NT}} = |\vec{T}\times\vec{L}| = \frac{3\sqrt{3}a^2}{2}|m_2 l_1 - m_1 l_2|. \tag{24}$$

Therefore, the number of atoms per unit cell in a carbon nanotube is given by

$$N_{\mathrm{NT}} = 2\frac{|\vec{T}\times\vec{L}|}{S} = 2|m_2 l_1 - m_1 l_2|. \tag{25}$$

For nanotubes of considerably large dimensions, the energy bands can be obtained by simply imposing periodic boundary conditions on the wavefunctions along the circumferential direction: $\Psi(\vec{x} + \vec{L}) = \Psi(\vec{x})$ [10]. In the first quantization formalism, the solutions of Equation (11), in real space, should obey the conditions $\psi_{\vec{K},\sigma}(\vec{x} + \vec{L}) = \psi_{\vec{K},\sigma}(\vec{x})$ and $\psi_{\vec{K}',\sigma}(\vec{x} + \vec{L}) = \psi_{\vec{K}',\sigma}(\vec{x})$, so that the respective translation operators, $e^{i(\vec{K}+\vec{p})\cdot\vec{L}}$ and $e^{i(\vec{K}'+\vec{p}')\cdot\vec{L}}$, give the conditions $(\vec{K} + \vec{p})\cdot\vec{L} = 2\pi l$ for $\psi_{\vec{K},\sigma}(\vec{x})$ and $(\vec{K}' + \vec{p}')\cdot\vec{L} = 2\pi l'$ for $\psi_{\vec{K}',\sigma}(\vec{x})$, with $l, l' \in \mathbb{Z}$ [21]. Since $\vec{K}\cdot\vec{L} = \frac{2\pi i}{3}[l_1 + l_2] = \frac{2\pi i\nu}{3}$ and $\vec{K}'\cdot\vec{L} = -\frac{2\pi i}{3}[l_1 + l_2] = -\frac{2\pi i\nu}{3}$, where ν may take the values $-1, 0, +1$ and is determined by the relation $l_1 + l_2 = 3n + \nu$ involving integer numbers only, the allowed values for the momenta p_L and p'_L along the circumference direction are given by the following:

$$p_L = \frac{2\pi l}{L} - \frac{2\pi\nu}{3L} \quad \text{and} \quad p'_L = \frac{2\pi l'}{L} + \frac{2\pi\nu}{3L}. \tag{26}$$

Due to discretization of the momentum component along the direction of $\vec{L}$, after rolling into a cylinder, the two-dimensional energy bands of graphene are reduced to a set of one-dimensional bands, for which energy is a function of p_T for each permitted value of p_L. The structure of the energy bands of a given carbon nanotube depends considerably on whether the points $\vec{K}$ and $\vec{K}'$ of the graphene reciprocal lattice are included in the set of allowed momenta for the nanotube. This can be clearly seen if one analyzes the dispersion

relation in the vicinity of the Fermi level, Equation (10), for which the discrete values of the momenta along the circumference give a band gap of $\frac{4\pi|\nu|v_F}{3L}$.

Translation parallel to the tube axis by a distance T gives the following relations for plane waves with momenta $\vec{K}$ and $\vec{K}'$:

$$\begin{aligned} e^{i\vec{K}\cdot\vec{T}}\psi_{\vec{K},\sigma}(\vec{x}) &= e^{iK_T T}\psi_{\vec{K},\sigma}(\vec{x}) = e^{\frac{2\pi i\mu}{3}}\psi_{\vec{K},\sigma}(\vec{x}) \,, \\ e^{i\vec{K}'\cdot\vec{T}}\psi_{\vec{K}',\sigma}(\vec{x}) &= e^{-iK'_T T}\psi_{\vec{K}',\sigma}(\vec{x}) = e^{-\frac{2\pi i\mu}{3}}\psi_{\vec{K}',\sigma}(\vec{x}) \,, \end{aligned} \tag{27}$$

so that the coordinates K_T and K'_T of graphene's reciprocal lattice are mapped onto $K_{\mathrm{NT}} = 2\pi\mu/3T$ and $K'_{\mathrm{NT}} = -2\pi\mu/3T$, respectively, where $\mu \in \{-1, 0, +1\}$.

For an arbitrary choice of the chiral vector $\vec{L}$ the nanotube can have either a chiral or helical structure. Amongst the possible non-chiral configurations, two possibilities are of special interest: zigzag, for which $\vec{L} = m\vec{a}_1$, $\vec{L} = m\vec{a}_2$ or $\vec{L} = m(\vec{a}_1 + \vec{a}_2)$, and armchair, for which $\vec{L} = 2m\vec{a}_1 + m\vec{a}_2$.

A nanotube with zigzag configuration will keep the conducting properties of flat graphene if m is a multiple of 3 (and thus $\nu = 0$), otherwise it will present a band gap. The translation vector along the tube axis may assume three equivalent forms, corresponding to the three aforementioned choices of $\vec{L}$, all of which have a module of $|\vec{T}| = 3a$ and, when multiplied by $\vec{K}'$ or $\vec{K}$, give $\mu = 0$, resulting in $K_{\mathrm{NT}} = K'_{\mathrm{NT}} = 0$.

Armchair nanotubes always present graphene-like conducting properties, since $\nu = 0$ for any choice of m. The translation vector through the cylinder axis has the form $\vec{T} = \vec{a}_2$ and the points $\vec{K}$ and $\vec{K}'$ are mapped onto $K_{\mathrm{NT}} = 2\pi/3\sqrt{3}a$ and $K'_{\mathrm{NT}} = -2\pi/3\sqrt{3}a$, respectively. The parameters characterizing zigzag and armchair configurations are summarized in Table 1.

Table 1. Parameters characterizing zigzag and armchair nanotubes.

Type	l_1	l_2	ν	m_1	m_2	T	μ	K_{NT}	K'_{NT}
Zigzag	m	0	0	1	2	$3a$	0	0	0
	m	0	±1	1	2	$3a$	0	0	0
	m	m	0	-1	1	$3a$	0	0	0
	m	m	±1	-1	1	$3a$	0	0	0
	0	m	0	-2	-1	$3a$	0	0	0
	0	m	±1	-2	-1	$3a$	0	0	0
Armchair	$2m$	m	0	0	1	$\sqrt{3}a$	1	$\frac{2\pi}{3\sqrt{3}a}$	$-\frac{2\pi}{3\sqrt{3}a}$

When a magnetic flux is applied along the nanotube's cross section, the momenta calculated from the points $\vec{K}$ and $\vec{K}'$ experience a shift of the form $\vec{p} \to \vec{p} - e\vec{A}$, so that, after translation by $\vec{L}$, the wavefunctions acquire an extra phase factor dependent on the the magnetic flux [10,19] and $p_L \to \frac{2\pi}{L}(l - \phi \pm \frac{\nu}{3})$, where $\phi = \Phi/\Phi_0 = e\vec{A}\cdot\vec{L}/2\pi$ (In fact, $\Phi = \oint \vec{A}\cdot \mathrm{d}\vec{l}$ over the contour L. However, in the limit of the slowly varying field $\vec{A}$, one can suppose that $\Phi \approx \vec{A}\cdot\vec{L}$.) and the plus sign corresponds to $\vec{K}'$, while the minus corresponds to $\vec{K}$.

2.3. Reduced Lagrangian for the Gauge Field

The action functional for massless fermions in a D-dimensional ($D = d + 1$) Minkowski space-time in the presence of an external electromagnetic field is given in quantum electrodynamics by the following expression [22]:

$$S = \int \left[-\frac{1}{4}F'_{\mu\nu}F'^{\mu\nu} - \frac{1}{2\xi}(\partial_\mu A'^{\mu})^2 + i\overline{\Psi}\gamma^\mu D'_\mu \Psi \right] \mathrm{d}^D X \,, \tag{28}$$

$$F'_{\mu\nu} = \partial_\mu A'_\nu - \partial_\nu A'_\mu \,, \qquad D'_\mu = \partial_\mu + ieA_\mu + ieA'_\mu \,, \tag{29}$$

where $X^\mu = (x^0, x^1, \ldots, x^d)$, and A^μ and A'^μ are, respectively, the external and the generated (by fermions) eletromagnetic fields in D-dimensional space-time ($\mu, \nu = \overline{0, d}$). In view of the explicit representation of the Lorentz invariance of the action functional, the Lorentz gauge was chosen with an arbitrary value of parameter ξ.

After extracting from the covariant derivative, the interaction of the fermions with the generated gauge field and expressing this respective term through the current, $\overline{\Psi}\gamma^\mu\Psi = J'^\mu$, one obtains for the action

$$S = \int \left\{ \frac{1}{2} A'^\mu \underbrace{\left[\partial^2 g_{\mu\nu} - \left(1 - \frac{1}{\xi}\right) \partial_\mu \partial_\nu \right]}_{\hat{G}_{\mu\nu}} A'^\nu - e J'_\mu A'^\mu + i\overline{\Psi}\gamma^\mu D_\mu \Psi \right\} \mathrm{d}^D X \,. \tag{30}$$

where $D_\mu = \partial_\mu + ieA_\mu$. Using the method of stationary point, the configuration of the field A'^μ which minimizes the action is given by the solution of the differential equation $\hat{G}_{\mu\nu} A'^\nu_{\text{ext}} = e J'_\mu$. The Green's function for this equation in D-dimensional momentum space has the well known form

$$D_0^{\nu\sigma}(K) = -\frac{g^{\nu\sigma}}{K^2} + \frac{(1-\xi) K^\nu K^\sigma}{(K^2)^2} \,, \tag{31}$$

In a reduced quatum field theory on a d'-brane, one can assume that the fermionic current has the form [17]

$$\begin{cases} J'^\mu(X) = 0 & \text{if } \mu = d'+1, d'+2, \ldots, d \\ J'^\mu(X) = j'^\mu(x)\delta^{d-d'}(\overline{x}) & \text{if } \mu = \overline{0, d'} \end{cases} , \tag{32}$$

where x and $\overline{x}$ represent the vectors $x^\alpha = (x^0, x^1, \ldots, x^{d'})$ and $\overline{x}^\zeta = (x^{d'+1}, x^{d'+2}, \ldots, x^d)$, respectively. Furthermore, since fermions are located on the brane, the fermionic terms in the Lagrangian related to the extra $d - d'$ degrees of freedom can be neglected.

By using the expressions (31) and (32) in the action functional and integrating over $\overline{x}$ and $\overline{y}$, one obtains

$$S_{\text{eff}} = \int \left\{ \int \left[-\frac{e^2}{2} j'_\alpha(x) D_0^{\alpha\beta}(x - y; \overline{x} - \overline{y} = 0) j'_\beta(y) \right] \mathrm{d}^{d'+1} y + i\overline{\Psi}\gamma^\alpha D_\alpha \Psi \right\} \mathrm{d}^{d'+1} x \,, \tag{33}$$

where $\alpha, \beta = \overline{0, d'}$ and the reduced Green's function is given by the following:

$$D_{0\ (d\to d')}^{\alpha\beta}(x - y) = \int e^{-ik(x-y)} \left(-\frac{g^{\alpha\beta}}{k^2 + \overline{k}^2} + \frac{(1-\xi) k^\alpha k^\beta}{(k^2 + \overline{k}^2)^2} \right) \frac{\mathrm{d}^{d'+1} k \, \mathrm{d}^{d-d'} \overline{k}}{(2\pi)^D} \,. \tag{34}$$

The vector $\overline{k}$ is space-like in the Minkowski metric.

For the reduction from a $(3+1)$-dimensional sytem to a $(3+1)$-dimensional one, integration over $\overline{k} = k^3$ gives the following:

$$D_{0\ (3\to 2)}^{\alpha\beta}(x - y) = -i \int e^{-ik(x-y)} \left(-\frac{g^{\alpha\beta}}{k^2} + \frac{(1-\xi') k^\alpha k^\beta}{(k^2)^2} \right) \frac{\sqrt{k^2}}{2} \frac{\mathrm{d}^3 k}{(2\pi)^3} \,, \tag{35}$$

in which $\alpha, \beta = \overline{0, 2}$ and the substition $\xi \to 2\xi' - 1$ was done.

Equation (35) actually resembles the one given in (31): $D_0^{\alpha\beta}(k) = 2i D_{0\ (3\to 2)}^{\alpha\beta}(k)/\sqrt{k^2}$, if one ignores the difference in the dimensions of the arguments and tensor indices. Since the propagator (35) corresponds to the inverse of the operator $\hat{G}_{\mu\nu}$, expression (35) should correspond to the inverse of the following operator:

$$\frac{2i\hat{G}_{\alpha\beta}}{\sqrt{-\partial^2}} = -2i\sqrt{-\partial^2} g_{\alpha\beta} - 2i\left(1 - \frac{1}{\xi'}\right) \frac{\partial_\alpha \partial_\beta}{\sqrt{-\partial^2}} \tag{36}$$

and thus the $(2+1)$-dimensional reduced action has the following form ($\alpha, \beta = \overline{0,2}$) [17]:

$$S_{\text{eff}} = \int \left[-\frac{1}{2} F'_{\text{red}\,\alpha\beta} \frac{1}{\sqrt{\partial^2}} F'^{\alpha\beta}_{\text{red}} - \frac{1}{\xi'} \partial_\alpha A'^{\alpha}_{\text{red}} \frac{1}{\sqrt{\partial^2}} \partial_\beta A'^{\beta}_{\text{red}} - e j'_\alpha A'^{\alpha}_{\text{red}} + i\overline{\Psi}\gamma^\alpha D_\alpha \Psi \right] \mathrm{d}^3 x \,. \quad (37)$$

3. Induced Current and Aharonov–Bohm Effect in Nanotubes

If one ignores the field A'^{α} and considers the external electromagnetic field as constant on the surface of graphene, the generating functional can be found without resorting to perturbative methods [23]:

$$Z = \int \exp\left\{ \int_0^\beta \int \overline{\Psi}_\sigma \left[-\gamma^0 \left(\frac{\partial}{\partial \tau} + ieA_0 - \mu \right) + iv_F \vec{\gamma} \cdot \left(\vec{\partial} - ie\vec{A} \right) \right] \Psi_\sigma \, \mathrm{d}^2 x \, \mathrm{d}\tau \right\} i \, \mathrm{d}\Psi^\dagger \, \mathrm{d}\Psi \,, \quad (38)$$

which, on the other hand, can be expressed as $Z = \exp[-NS_T \beta V_{\text{eff}}]$, where S_T is the area of the two-dimensional space, N is the number of flavours, including both spin degrees of freedom and the number of layers (for multiwalled nanotubes), and V_{eff} is the effective potential.

With the help of the Fourier series, the fermionic wavefunctions can be expanded as ($\omega_n = (2n+1)\pi T$)

$$\Psi(\vec{x})_\sigma = \sqrt{1/S_T} \sum_{\vec{p}} \sum_n \exp(i\omega_n \tau + i\vec{p} \cdot \vec{x}) \Psi_n(\vec{p}) \,, \quad (39)$$

$$\overline{\Psi}_\sigma(\vec{x}) = \sqrt{1/S_T} \sum_{\vec{p}} \sum_n \exp(-i\omega_n \tau - i\vec{p} \cdot \vec{x}) \overline{\Psi}_n(\vec{p}) \,, \quad (40)$$

so that one can easily compute the path integral for the generating functional

$$Z = \prod_{\sigma=1}^{N} \prod_n \prod_{\vec{p}} \left\{ \beta^2 \left[(\Omega_n + i\mu)^2 + v_F^2 \vec{P}^2 \right] \right\}^2 , \quad (41)$$

where $\Omega_n = \omega_n + eA_0$, $\vec{P} = \vec{p} - e\vec{A}$.

If the Zeeman effect is not accounted for, the effective potential takes the following form for continuous momenta:

$$V_{\text{eff}} = -2T \sum_n \int \ln \left\{ \beta^2 \left[\left(\frac{2\pi}{\beta} \right)^2 \left(n + \frac{1}{2} + \frac{\beta}{2\pi} [eA_0 + i\mu] \right)^2 + v_F^2 \vec{P}^2 \right] \right\} \frac{\mathrm{d}^2 p}{(2\pi)^2} . \quad (42)$$

In the cylindrical coordinate system, in which the cylinder axis is parallel to the considered graphene sheet and the magnetic field has the form $\vec{H} = H\vec{e}_z$, the configuration of the vector potential may be chosen as a null radial component ($A_\rho = 0$) and an azimuthal component $A_\theta = H\rho/2$. If one then assumes that both chemical and electric potentials equal zero and apply periodic boundary conditions on the graphene wavefunction along the direction perpendicular to the magnetic field ($\Psi(x_2 + 2\pi R) \to \Psi(x_2)$, $p_1 \to p_z$, $p_2 \to p_\theta = 2\pi l/L$), which is equivalent to rolling up the graphene sheet into a tube, considering $\nu = 0$, the result reads as follows:

$$V_{\text{eff}} = \frac{-2T}{L} \sum_n \sum_l \int \ln \left\{ \beta^2 \left[\left(\frac{2\pi}{\beta} \right)^2 \left(n + \frac{1}{2} \right)^2 + v_F^2 p_1^2 + \left(\frac{2\pi v_F}{L} \right)^2 (l - \phi)^2 \right] \right\} \frac{\mathrm{d}p_1}{2\pi} \,, \quad (43)$$

where $\phi = LeA_\theta/2\pi = LeHR/4\pi$ ($R = L/2\pi$ is the cylinder radius). At zero temperature ($\beta \to \infty$), the effective potential (43) can be written as

$$V_{\text{eff},0} = \lim_{T \to 0} \frac{-2}{L v_F} \sum_{l=-\infty}^{\infty} \int_0^{2\pi} \int_0^\infty \ln \left\{ \left[p^2 + \left(\frac{2\pi v_F}{L} \right)^2 (l - \phi)^2 \right] T^{-2} \right\} \frac{p \, \mathrm{d}p \, \mathrm{d}\theta}{(2\pi)^2} \,, \quad (44)$$

with $p^2 = p_0^2 + v_F^2 p_1^2$ and $\theta = \arctan(v_F p_1 / p_0)$.

Using the formula

$$\ln \frac{A}{B} = -\int_0^\infty \frac{e^{-sA} - e^{-sB}}{s}\, \mathrm{d}s\,, \tag{45}$$

it is possible to obtain, after integration over p^2,

$$V_{\mathrm{eff},0} = \frac{1}{2\pi L v_F} \sum_{l=-\infty}^{\infty} \int_0^\infty \exp\left[-s\left(\frac{2\pi v_F}{L}\right)^2 (l-\phi)^2 \right] \frac{\mathrm{d}s}{s^2} + \dots\,. \tag{46}$$

The three dots in Equation (46) account for infinite terms, which do not bring any meaningful contribution to the effective potential. Formula (47) enables us to write the potential (46) in a more convenient form for further calculations [24]:

$$\sum_{l=-\infty}^{\infty} \exp\left[-s\left(\frac{2\pi l}{B} + C\right)^2 \right] = \frac{B}{2\sqrt{\pi s}} \left[1 + 2\sum_{l=1}^{\infty} \exp\left(\frac{-B^2 l^2}{4s}\right) \cos(BCl) \right]. \tag{47}$$

Consequently,

$$V_{\mathrm{eff},0} = \frac{1}{4\pi^{3/2} v_F^2} \int_0^\infty \left[1 + 2\sum_{l=1}^{\infty} \exp\left(\frac{-L^2 l^2}{4 v_F^2 s}\right) \cos(2\pi l \phi) \right] \frac{\mathrm{d}s}{s^{5/2}} + \dots\,. \tag{48}$$

The part of the integrand in expression (48) containing the summation operator is the only one to contribute to the induced current. Ignoring the remaining terms, and upon integrating over s, the potential reads

$$V_{\mathrm{eff},0} = \frac{2 v_F}{\pi L^3} \sum_{l=1}^{\infty} \frac{1}{l^3} \cos(2\pi l \phi) + \dots\,. \tag{49}$$

Finally, one can achieve a simple expression for the induced current. The latter can be obtained through differentiation of the effective potential relative to the azimuthal component of the vector potential

$$e j_0 = \frac{\partial V_{\mathrm{eff},0}}{\partial A_\theta} = \frac{Le}{2\pi} \frac{\partial V_{\mathrm{eff},0}}{\partial \phi} = -\frac{2 e v_F}{\pi L^2} \sum_{l=1}^{\infty} \frac{1}{l^2} \sin(2\pi l \phi)\,, \tag{50}$$

and it has the same direction as the only non-zero component of the vector potential, A_θ. The infinite sum in expression (50) has a well-defined value

$$j_0 = \frac{i v_F}{\pi L^2} \left[\mathrm{Li}_2(e^{2i\pi\phi}) - \mathrm{Li}_2(e^{-2i\pi\phi}) \right]. \tag{51}$$

Figure 3 shows the dependence of the induced current j_0 on the magnetic flux ϕ for a nanotube with $L = 100$ Å. Differently from what can be expected in the classical case, the adiabatic increase of the magnetic field intensity results in an oscillatory behaviour for the current, so that, for each interval $\phi \in [m, m+1)$ with $m \in \mathbb{Z}$, it changes its sign at the point $\phi = m + 1/2$.

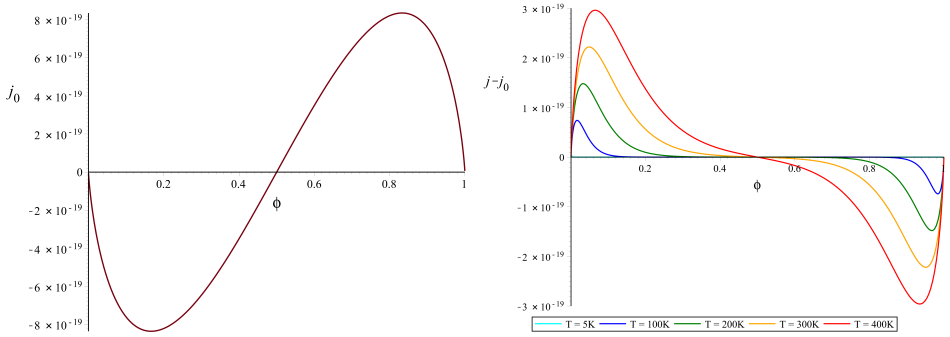

Figure 3. Left: Induced current j_0 as a function of ϕ for $L = 100$ Å. **Right**: Temperature effects on induced current $j - j_0$ as a function of ϕ for $L = 100$ Å. The abscissa is given in units of GeV^2.

The effects arising solely from finite temperature (holding $\mu = 0$) can be accounted for in a similar way. Equation (43) can be simplified using formulas (45) and (47) and integrating over p_1

$$V_{\text{eff}} = \frac{1}{4\pi^{3/2}v_F^2}\int_0^\infty [1 + 2\sum_{l=1}^{\infty}\exp(\frac{-L^2l^2}{4v_F^2 s})\cos(2\pi l\phi)][1 + 2\sum_{n=1}^{\infty}\exp(\frac{-\beta^2n^2}{4s})\cos(n\pi)]\frac{\mathrm{d}s}{s^{5/2}}\,. \quad (52)$$

The corresponding induced current can be obtained from expression (52) after integration over s and differentiation with respect to A_θ

$$ej = \frac{\partial V_{\text{eff}}}{\partial A_\theta} = -\frac{2ev_F}{\pi L^2}\sum_{l=1}^{\infty}\frac{1}{l^2}\sin(2\pi l\phi) - \frac{4Lev_F}{\pi}\sum_{l=1}^{\infty}\sum_{n=1}^{\infty}\frac{(-1)^n l}{(L^2l^2 + \beta^2v_F^2n^2)^{3/2}}\sin(2\pi l\phi)\,. \quad (53)$$

The resulting currents with $\mu = 0$ are shown in Figure 3, where both summations were performed up to the 999th term. Computational calculations have shown that the result of such a double sum converges considerably rapidly for the chosen value of the circumference, $L = 100$ Å, so that there was no visible difference in the results obtained having 600 or more as the upper summation limit. In terms of absolute values, the total induced current decreases with increasing temperature, so that a complete damping of the induced current would be theoretically expected at infinite temperature (it should be noted that nanotubes start to burn around 700°C [25]) (see Figure 4).

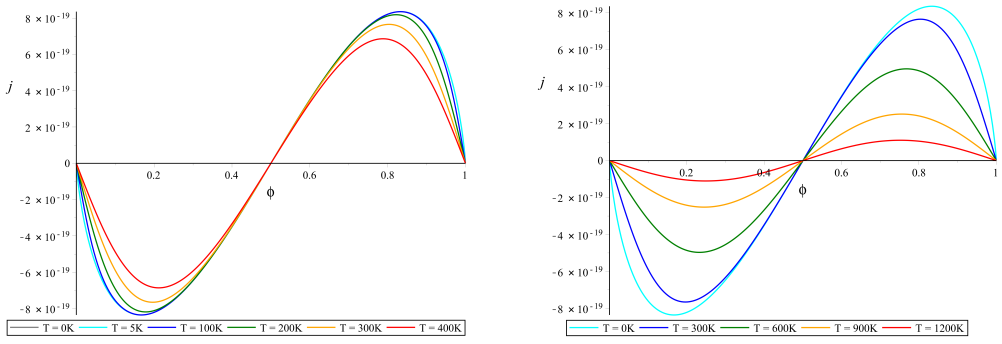

Figure 4. Total induced current for $\mu = 0$. **Left**: total induced current for the temperature interval from 0 K to 400 K. For temperatures from 0 K to 100 K the difference is almost not seen in the plot. **Right**: Total induced current for the temperature interval from 0 K to 1200 K. Current given in units of GeV^2.

If one accounts for the non-zero chemical potential ($\mu \neq 0$), the approach preesnted above does not allow for the removal of all divergences related to terms containing μ. For this purpose, one can start from Equation (43) and take into account the chemical potential

$$V_{\text{eff}} = \frac{-2T}{L}\sum_{n=-\infty}^{\infty}\sum_{l=-\infty}^{\infty}\int_{-\infty}^{\infty}\ln\left\{\beta^2\left[\left(\frac{2\pi}{\beta}\right)^2\left(n+\frac{1}{2}+\frac{i\beta\mu}{2\pi}\right)^2+v_F^2p_1^2+\left(\frac{2\pi v_F}{L}\right)^2(l-\phi)^2\right]\right\}\frac{\mathrm{d}p_1}{2\pi}\,. \quad (54)$$

The summation over the index n in $\omega_n = (2n+1)\pi T$ can be substituted by integration over ω in the space of complex numbers, with the integrand modulated by the function $(i/2)\tan(\beta\omega/2)$, for which the poles are localized at the points $\omega = \omega_n$. In view of the localization of the modulating function poles along the axis of real ω, the contour of integration can be taken so as to enclose the poles along the real axis counter-clockwise:

$$V_{\text{eff}} = \frac{-T}{\pi L}\sum_{l=-\infty}^{\infty}\int_{-\infty}^{\infty}\int_{T^2}^{\left[v_F^2p_1^2+\left(\frac{2\pi v_F}{L}\right)^2(l-\phi)^2\right]}\oint\frac{1}{\theta^2+(\omega+i\mu)^2}\frac{i\tan(\frac{\beta\omega}{2})}{2}\frac{\mathrm{d}\omega}{2\pi T}\,\mathrm{d}\theta^2\,\mathrm{d}p_1\,. \quad (55)$$

However, the integrand in expression (55) still contains two poles in the imaginary axis: $i(\theta-\mu)$ and $-i(\theta+\mu)$. Consequently, the contour of integration can be deformed, in order to close the contour under the axis of real values $\Re(\omega)$, with a clockwise-oriented semi-circle in the infinity of the half-plane $\Im(\omega) < 0$, while the contour above the abscissa axis $\Re(\omega)$ is closed by a clockwise-oriented semi-circle in the infinity of the half-plane $\Im(\omega) > 0$. The theorem of residues gives

$$V_{\text{eff}} = \frac{-1}{L}\sum_{l=-\infty}^{\infty}\int_{-\infty}^{\infty}\int_{T}^{\sqrt{v_F^2p_1^2+\left(\frac{2\pi v_F}{L}\right)^2(l-\phi)^2}}\left\{\tanh\left[\frac{\beta}{2}(\theta-\mu)\right]+\tanh\left[\frac{\beta}{2}(\theta+\mu)\right]\right\}\mathrm{d}\theta\frac{\mathrm{d}p_1}{2\pi}\,. \quad (56)$$

By integrating expression (56) over θ and discarding the infinite terms, one obtains

$$\begin{aligned} V_{\text{eff}} = \frac{-2}{\beta L}\sum_{l=-\infty}^{\infty}\int_{-\infty}^{\infty}\Bigg\{&\beta\sqrt{v_F^2p_1^2+\left(\frac{2\pi v_F}{L}\right)^2(l-\phi)^2}+\\ &\ln\left\{1+\exp\left[-\beta\left(\sqrt{v_F^2p_1^2+\left(\frac{2\pi v_F}{L}\right)^2(l-\phi)^2}-\mu\right)\right]\right\}+\\ &\ln\left\{1+\exp\left[-\beta\left(\sqrt{v_F^2p_1^2+\left(\frac{2\pi v_F}{L}\right)^2(l-\phi)^2}+\mu\right)\right]\right\}\Bigg\}\frac{\mathrm{d}p_1}{2\pi}\,. \end{aligned} \quad (57)$$

In the limit of zero temperature expression, (57) gives the known Equation (44) with the help of Formula (58)

$$\int\ln[\beta^2(p_0^2+E^2)]\frac{\mathrm{d}p_0}{2\pi} = E+\dots\,, \quad (58)$$

in which E represents the integrant from expression (57) after aplying the limit $\beta\to\infty$. The differentiation of Equation (57) with respect to the field A_θ gives the induced current for non-zero T and μ

$$\begin{aligned} j-j_0 = -\sum_{l=-\infty}^{\infty}\int_{-\infty}^{\infty}\Bigg\{&\frac{1}{1+\exp\left[\beta\left(\sqrt{v_F^2p_1^2+\left(\frac{2\pi v_F}{L}\right)^2(l-\phi)^2}-\mu\right)\right]}+\\ &\frac{1}{1+\exp\left[\beta\left(\sqrt{v_F^2p_1^2+\left(\frac{2\pi v_F}{L}\right)^2(l-\phi)^2}+\mu\right)\right]}\Bigg\}\frac{\left(\frac{2\pi v_F}{L}\right)^2(l-\phi)}{\sqrt{v_F^2p_1^2+\left(\frac{2\pi v_F}{L}\right)^2(l-\phi)^2}}\frac{\mathrm{d}p_1}{2\pi^2}\,. \end{aligned} \quad (59)$$

The accounting of the Zeeman effect is carried out by adding to the chemical potential a term of the form $-gs\mu_B H/2 = -4\pi^2 gs\mu_B \phi/L^2 e$ and substituting the coefficient 2 before the integral for a summation over s ($2 \to \sum_{s=-1/2}^{+1/2}$) in Equation (57)

$$V_{\text{eff}} = \frac{-1}{\beta L} \sum_{s=-1/2}^{+1/2} \sum_{l=-\infty}^{\infty} \int_{-\infty}^{\infty} \left\{ \beta \sqrt{v_F^2 p_1^2 + \left(\frac{2\pi v_F}{L}\right)^2 (l-\phi)^2} + \right.$$
$$\ln\left\{1 + \exp\left[-\beta\left(\sqrt{v_F^2 p_1^2 + \left(\frac{2\pi v_F}{L}\right)^2 (l-\phi)^2} - \mu_s\right)\right]\right\} +$$
$$\left. \ln\left\{1 + \exp\left[-\beta\left(\sqrt{v_F^2 p_1^2 + \left(\frac{2\pi v_F}{L}\right)^2 (l-\phi)^2} + \mu_s\right)\right]\right\}\right\} \frac{\mathrm{d}p_1}{2\pi}\,, \tag{60}$$

where $\mu_s = \mu - 4\pi^2 gs\mu_B \phi/L^2 e$. The part of the current that depends on μ, T and on the Zeeman effect has the form ($e \to \sqrt{\alpha}$)

$$j - j_0 = -\sum_{l=-\infty}^{\infty} \int_{-\infty}^{\infty} \left\{ \frac{\left(\frac{2\pi v_F}{L}\right)^2 (l-\phi)\left[v_F^2 p_1^2 + \left(\frac{2\pi v_F}{L}\right)^2 (l-\phi)^2\right]^{-1/2} - \frac{2\pi^2 g\mu_B}{\sqrt{\alpha} L^2}}{1 + \exp\left[\beta\left(\sqrt{v_F^2 p_1^2 + \left(\frac{2\pi v_F}{L}\right)^2 (l-\phi)^2} - \mu + \frac{2\pi^2 g\mu_B \phi}{\sqrt{\alpha} L^2}\right)\right]} + \right.$$
$$\frac{\left(\frac{2\pi v_F}{L}\right)^2 (l-\phi)\left[v_F^2 p_1^2 + \left(\frac{2\pi v_F}{L}\right)^2 (l-\phi)^2\right]^{-1/2} + \frac{2\pi^2 g\mu_B}{\sqrt{\alpha} L^2}}{1 + \exp\left[\beta\left(\sqrt{v_F^2 p_1^2 + \left(\frac{2\pi v_F}{L}\right)^2 (l-\phi)^2} - \mu - \frac{2\pi^2 g\mu_B \phi}{\sqrt{\alpha} L^2}\right)\right]} +$$
$$\left. \frac{\left(\frac{2\pi v_F}{L}\right)^2 (l-\phi)\left[v_F^2 p_1^2 + \left(\frac{2\pi v_F}{L}\right)^2 (l-\phi)^2\right]^{-1/2} - \frac{2\pi^2 g\mu_B}{\sqrt{\alpha} L^2}}{1 + \exp\left[\beta\left(\sqrt{v_F^2 p_1^2 + \left(\frac{2\pi v_F}{L}\right)^2 (l-\phi)^2} + \mu + \frac{2\pi^2 g\mu_B \phi}{\sqrt{\alpha} L^2}\right)\right]} \right\} \frac{\mathrm{d}p_1}{4\pi^2}\,. \tag{61}$$

Experimental measurements of the electrical resistivity in multiwalled nanotubes, in the presence of an axial magnetic flux through the tube section (Aharonov–Bohm effect), show that the increase in the intensity of the magnetic flux causes oscillations in the measured quantity, which reaches its maximum at $\phi = 0$ and then varies periodically with maxima at points $\Phi = m\Phi_0/2$ ($m \in \mathbb{Z}$) and valleys therebetween [15,16]. The increase in temperature provokes a damping of the oscillations, reducing the maximal resistivity but keeping the period unchanged. Furthermore, the electrical resistivity was found to be practically independent of the nanotubes' length, while the current in general flows through the outermost walls of multiwalled nanotubes, pointing to a small current conductivity between the concentric layers and to the equality between the mean current-carrying radius (effective radius) and the radius of the outermost tube [15,25]. Those results are qualitatively in agreement with the results obtained in the present work, according to which the induced current should oscillate with zeros at points $\phi = \Phi/\Phi_0 = m/2$ and maxima (in absulute value) at $\phi \approx m \pm 0, 2$, with amplitude dampings being expected for higher temperatures.

The physical explanation for the obtained results is possible with the help of the Aharonov–Bohm effect and Hall effect theories. The process is similar to what happens with a metallic ring, through which a magnetic flux flows confined to an axial solenoid. During the adiabatic process of turning on the magnetic flux, the surging electric field transfers angular momentum to the electrons. Consequently, the eigenstates of the ring evolve under the influence of the electric field, changing their energy. The electrons in the former ground state of the system remain in this same state due to the adiabaticity of the

process, even though this state may not be the ground state for the system in the presence of an electric field. During this process, it is possible that states with varying energies achieve a common energy value and become degenerate. However, the appearance of degeneracies does not allow electronic transitions between these momentarily degenerate states, since the states correspond to different canonical angular momenta and the electronic transition would go against the law of conservation of angular momentum [26].

As a result of the adiabatic process of turning on the magnetic flux in nanotubes, the new ground state can be a state, for which the current is non-zero. The further adiabatic increase of the magnetic flux up to $\phi = 1/2$ can gradually lead to a state similar to the former ground state for $\phi = 0$, but for which the valence and conduction bands are interchanged. This enables one to explain the inversion of the current for $1/2 < \phi < 1$, where the evolution of states would take place in the opposite direction to that which is seen for $0 < \phi < 1/2$. This behavior should repeat itself periodically with the increase in ϕ due to the Aharonov–Bohm effect.

4. Summary and Conclusions

The induced current derived from an effective potential approach in the formalism of finite-temperature quantum field theory revealed itself to have quite a peculiar oscillatory behavior in the presence of the Aharonov–Bohm effect. The amplitude of these oscillations is damped by temperature, while the period remains unchanged. Perturbative corrections, accounting for the limited degrees of freedom of photons, can be made in a similar way to the already known Feynman rules for finite-temperature quantum electrodynamics and give minor current oscillations with reduced period and amplitude.

Funding: This research received no external funding.

Data Availability Statement: Not applicable.

Acknowledgments: The author is grateful to T.L.M. Guedes and P.B. Kolmakov, who helped greatly in preparing some of the results discussed in this paper.

Conflicts of Interest: The authors declare no conflict of interest.

References

1. Fradkin, E. *Field Theories of Condensed Matter Systems*; Addison-Wesley Publishing Company: Reading, MA, USA, 1991.
2. Nagaosa, N. *Quantum Field Theory in Condensed Matter Physics*; Springer: Berlin/Heidelberg, Germany, 1999.
3. Heeger, A.J.; Kivelson, S.; Schrieffer, J.R.; Su, W.-P. Solitons in conducting polymers. *Rev. Mod. Phys.* **1988**, *60*, 781. [CrossRef]
4. Campbell, D.K.; Bishop, A.R. Soliton excitations in polyacetylene and relativistic field theory models. *Nucl. Phys.* **1982**, *200*, 297–328. [CrossRef]
5. Shifman, M. *At the Frontier of Particle Physics: Handbook of QCD: "Boris Ioffe Festschrift"*; World Scientific: London, UK, 2001; Volume 3.
6. Neto, A.H.; Guinea, F.; Peres, N.M.R.; Novoselov, K.S.; Geim, A.K. The electronic properties of graphene. *Rev. Mod. Phys.* **2009**, *81*, 109. [CrossRef]
7. Novoselov, K.S.; Geim, A.K.; Morozov, S.V.; Jiang, D.; Zhang, Y.; Dubonos, S.V.; Grigorieva, I.V.; Firsov, A.A. Electric field effect in atomically thin carbon films. *Science* **2004**, *306*, 666–669. [CrossRef]
8. Novoselov, K.S.; Geim, A.K.; Morozov, S.V.; Jiang, D.; Katsnelson, M.I.; Grigorieva, I.V.; Dubonos, S.V.; Firsov, A.A. Two-dimensional gas of massless Dirac fermions in graphene. *Nature* **2005**, *438*, 197–200. [CrossRef]
9. Gusynin, V.P.; Sharapov, S.G.; Carbotte, J.P. AC conductivity of graphene: From tight-binding model to 2 + 1-dimensional quantum electrodynamics. *Int. J. Mod. Phys. B* **2007**, *21*, 4611–4658. [CrossRef]
10. Ando, T. Theory of Electronic States and Transport in Carbon Nanotubes. *J. Phys. Soc. Jpn.* **2005**, *74*, 777–817. [CrossRef]
11. Saito, R.; Fujita, M.; Dresselhaus, G.; Dresselhaus, M.S. Electronic structure of graphene tubules based on C60. *Phys. Rev. B* **1992**, *46*, 1804. [CrossRef]
12. Aharonov, Y.; Bohm, D. Significance of Electromagnetic Potentials in the Quantum Theory. *Phys. Rev.* **1959**, *115*, 485. [CrossRef]
13. Ebert, D.; Klimenko, K.G.; Kolmakov, P.B.; Zhukovsky, V.C. Phase transitions in hexagonal, graphene-like lattice sheets and nanotubes under the influence of external conditions. *Ann. Phys.* **2016**, *371*, 254–286. [CrossRef]
14. Stepanov, E.A.; Zhukovsky, V.C. Graphene under the influence of Aharonov-Bohm flux and constant magnetic field. *Phys. Rev. B* **2016**, *94*, 094101. [CrossRef]

15. Bachtold, A.; Strunk, C.; Salvetat, J.P.; Bonard, J.M.; Forró, L.; Nussbaumer, T.; Schönenberger, C. Aharonov–Bohm oscillations in carbon nanotubes. *Nature* **1999**, *397*, 673. [CrossRef]
16. Schönenberger, C.; Forró, L. Multiwall carbon nanotubes. *Phys. World* **2000**, *13*, 37. [CrossRef]
17. Gorbar, E.V.; Gusynin, V.P.; Miransky, V.A. Dynamical chiral symmetry breaking on a brane in reduced QED. *Phys. Rev. D* **2001**, *64*, 105028. [CrossRef]
18. Peskin, M.E.; Schroeder, D.V. *An Introduction to Quantum Field Theory*; CRC Press: Boca Raton, FL, USA, 1995.
19. Viet, N.A.; Ajiki, H.; Ando, T. Lattice instability in metallic carbon nanotubes. *J. Phys. Soc. Jpn.* **1994**, *63*, 3036–3047. [CrossRef]
20. Ajiki, H.; Ando, T. Electronic States of Carbon Nanotubes. *J. Phys. Soc. Jpn.* **1993**, *62*, 1255–1266. [CrossRef]
21. Charlier, J.C.; Blase, X.; Roche, S. Electronic and transport properties of nanotubes. *Rev. Mod. Phys.* **2007**, *79*, 677. [CrossRef]
22. Batalin, I.A.; Fradkin, E.S. Quantum electrodynamics in external fields. I. *Theor. Mat. Phys.* **1970**, *5*, 1080–1100. [CrossRef]
23. Kapusta, J.I.; Gale, C. *Finite-Temperature Field Theory: Principles and Applications*; Cambridge University Press: Cambridge, UK, 2006.
24. Ebert, D.; Zhukovsky, V.C.; Vshivtsev, A.S. Thermodynamic potential with condensate fields in an SU(2) model of QCD. *Intern. J. Mod. Phys. A* **1998**, *13*, 1723–1741. [CrossRef]
25. Frank, S.; Poncharal, P.; Wang, Z.L.; de Heer, W.A. Carbon Nanotube Quantum Resistors. *Science* **1998**, *280*, 1744–1746. [CrossRef]
26. Stern, A. Anyons and the quantum Hall effect—A pedagogical review. *Ann. Phys.* **2008**, *323*, 204–249. [CrossRef]

Disclaimer/Publisher's Note: The statements, opinions and data contained in all publications are solely those of the individual author(s) and contributor(s) and not of MDPI and/or the editor(s). MDPI and/or the editor(s) disclaim responsibility for any injury to people or property resulting from any ideas, methods, instructions or products referred to in the content.